ECCOMAS Congress 2016
VII European Congress on Computational Methods in Applied Sciences and Engineering
M. Papadrakakis, V. Papadopoulos, G. Stefanou, V. Plevris (eds.)
Crete Island, Greece, 5–10 June 2016

3D DRBEM MODELING FOR ROTATING INITIALLY STRESSED ANISOTROPIC FUNCTIONALLY GRADED PIEZOELECTRIC PLATES

Mohamed Abdelsabour Fahmy*, †

* Jummum University College
Umm Al-Qura University
Alazizya, behind Alsalam Souq, 21955 Makkah, Saudi Arabia.
e-mail: maselim@uqu.edu.sa, Web page: https://uqu.edu.sa/staff/ar/4340548

† Faculty of Computers and Informatics
Suez Canal University
New Campus, 4.5 Km, Ring Road, El Salam District, 41522 Ismailia, Egypt.
e-mail: Mohamed_fahmy@ci.suez.edu.eg
Web page: http://mohamed_fahmy_ci.staff.scuegypt.edu.eg

Keywords: Rotation, Initial Stress, Anisotropic, Functionally Graded Piezoelectric Plates, Dual Reciprocity Boundary Element Method.

Abstract. Functionally graded piezoelectric plates (FGPPs) considered in the current study have been received much attention in recent years due to their various applications including sensors and actuators, aerospace, nuclear energy, chemical plant, electronics, biomaterials, piezoelectric motors, reduction of vibrations and noise, infertility treatment, ultrasonic micromotors, micropumps and microvalves, photovoltaics.

The time-stepping dual reciprocity boundary element method modeling was proposed to study the 3D dynamic response of an anisotropic rotating initially stressed functionally graded piezoelectric plate (FGPP). The FGPP is assumed to be graded through the thickness. The main aim of this paper is to evaluate the effects of initial stress and rotation on the displacement components in an anisotropic FGPP. Then we studied the effect of inhomogeneity on the displacement components in presence of initial stress and rotation. In the end, the accuracy of the proposed method was examined and confirmed by comparing the obtained results with those known previously.

1. Introduction

Functionally graded piezoelectric plates (FGPPs) considered in the current study have been received much attention in recent years due to their various applications including sensors and actuators, aerospace, nuclear energy, chemical plant, electronics, biomaterials, piezoelectric motors, reduction of vibrations and noise, infertility treatment, ultrasonic micromotors, micropumps and microvalves, photovoltaics. Since it is very difficult to find the analytical solution to the considered problem, therefore, an important number of engineering and mathematical papers devoted to the numerical solution have been studied to describe the global behavior of such problems.

Piezoelectric ceramics are being widely used in electromechanical devices such as sensors, filters, ultrasonic generators and actuators because they offer excellent coupling properties between the mechanical and electrical fields of these devices, and the fracture of these piezoelectric materials has therefore been receiving a great deal of attention (Suo et al. [1], Pan [2], Jin and Zhong, [3], Zhang et al. [4], Lin et al. [5], Fang et al. [6], Abd-Alla and Al-Sheikh [7, 8], Kuna [9], Zaman et al. [10], Zhong et al. [11], Akbarzadeh et al. [12], Davì and Milazzo [13], Abd-Alla et al. [14], Abd-Alla and Askar [15], Alibeigloo and Liew [16] and Rafiee et al. [17]). It is well known that extension of the current fundamental fracture concepts and criteria from pure elasticity to piezoelectricity is not straightforward because of the coupling between the mechanical and electric fields.

The advantages in the boundary element method (BEM) arises from the fact that the BEM can be regarded as boundary–based method that uses the boundary integral equation formulations where only the boundary of the domain of the partial differential equation (PDE) is required to be meshed. But in the domain-based methods such the finite element method (FEM), finite difference method (FDM) and element free method (EFM) that use ordinary differential equation (ODE) or PDE formulations, where the whole domain of the PDE requires discretisation. Thus the dimension of the problem is effectively reduced by one, that is, surfaces for three–dimensional (3D) problems or curves for two-dimensional (2D) problems. And the equation governing the infinite domain is reduced to an equation over the finite boundary. Also, the BEM can be applied along with the other domain-based methods to verify the solutions to the problems that do not have available analytical solutions. Presence of domain integrals in the formulation of the BEM dramatically decreases the efficiency of this

technique. One of the most frequently used techniques for converting the domain integral into a boundary one is the so-called dual reciprocity boundary element method (DRBEM). This method was initially developed by Nardini and Brebbia [18] in the context of two-dimensional (2D) elastodynamics and has been extended to deal with a variety of problems wherein the domain integral may account for linear-nonlinear static-dynamic effects. A more extensive historical review and applications of dual reciprocity boundary element method may be found in Brebbia et al. [19], Wrobel and Brebbia [20], Partridge and Brebbia, [21], Partridge and Wrobel [22], Frijns et al. [23], Gaul [24] and Fahmy [25-34].

In this paper the governing equations of an anisotropic FGPP under the influence of gravity are solved by means of a time-stepping dual reciprocity boundary element method (DRBEM) to describe the displacement behavior of the homogeneous and functionally graded plates in an anisotropic FGPP under the influence of gravity. The accuracy of the proposed method was examined and confirmed by comparing the obtained results with those known previously.

2 FORMULATION OF THE PROBLEM

The governing equations for the stress wave propagation in anisotropic functionally graded piezoelectric plate may be written in the following form

$$\sigma_{fg,f} = \Gamma_{fg} + \rho(x+1)^m \ddot{u}_g + \rho(x+1)^m \omega^2 x_g \tag{1}$$

$$D_{f,f} = 0 \tag{2}$$

In which

$$\sigma_{fg} = (x+1)^m \left[C_{fghi}\varepsilon_{hi} - e_{ifg}E_i\right] \tag{3}$$

$$D_f = (x+1)^m \left[e_{fhi}\varepsilon_{hi} + \epsilon_{fi}E_i\right] \tag{4}$$

$$\Gamma_{fg} = P_0(x+1)^m \left(u_{g,f} - u_{f,g}\right) \tag{5}$$

where

$$\varepsilon_{hi} = \frac{1}{2}\left(u_{h,i} + u_{i,h}\right) \quad , \quad E_i = -\Phi_{,i} \tag{6}$$

Substituting (3)-(5) into (1) and (2) leads to

$$\left[C_{fghi}u_{h,if} + e_{ifg}\Phi_{,if}\right] + \frac{m}{x+1}\left[C_{fghi}u_{h,i} + e_{ifg}\Phi_{,i}\right] = \rho\ddot{u}_g$$
$$+P_0\left(u_{g,f} - u_{f,g}\right) + \rho\omega^2 x_g \tag{7}$$

$$\left[e_{fhi}u_{h,if} - \epsilon_{fi}\Phi_{,if}\right] + \frac{m}{x+1}\left[e_{fhi}u_{h,i} - \epsilon_{fi}\Phi_{,i}\right] = 0 \tag{8}$$

Where E_i is the electric field vector, Φ is the electric potential, D is the electric displacement, C_{fghi} is the elasticity tensor $\left(C_{fghi} = C_{gfhi} = C_{hifg}\right)$, e_{ifg} is the piezoelectric tensor $\left(e_{ifg} = e_{igf}\right)$, ϵ_{fi} is the permittivity tensor $\left(\epsilon_{fi} = \epsilon_{if}\right)$, ρ is the density and $\aleph = \frac{m}{x+1}$

A superposed dot denotes differentiation with respect to the time and a comma followed by a subscript denotes partial differentiation with respect to the corresponding coordinates.

The governing equations (7) and (8) can be written in the following form

$$C_{fghi}u_{h,if} = \rho\ddot{u}_g + P_0\left(u_{g,f} - u_{f,g}\right) + \rho\omega^2 x_g - C_{fghi}\aleph u_{h,i} - e_{ifg}\left[\Phi_{,if} + \aleph\Phi_{,i}\right] \tag{9}$$

$$e_{fhi}u_{h,if} = \epsilon_{fi}\Phi_{,if} - e_{fhi}\aleph u_{h,i} + \epsilon_{fi}\left[\Phi_{,if} + \aleph\Phi_{,i}\right] \tag{10}$$

3 NUMERICAL IMPLEMENTATION

The governing equations (9) and (10) can now be written in operator form as follows

$$L_{fg}u_h = b_{fg} \tag{11}$$

$$L_{fh}\Phi = b_{fh} \tag{12}$$

Where

$$L_{fg} = C_{fghi}\frac{\partial}{x_i}\frac{\partial}{x_f} \tag{13}$$

$$b_{fg} = \rho\ddot{u}_g + P_0\left(u_{g,f} - u_{f,g}\right) + \rho\omega^2 x_g - C_{fghi}\aleph u_{h,i} - e_{ifg}\left[\Phi_{,if} + \aleph\Phi_{,i}\right] \tag{14}$$

$$L_{fh} = e_{fhi}\frac{\partial}{x_i}\frac{\partial}{x_f} \tag{15}$$

$$b_{fh} = \epsilon_{fi}\Phi_{,if} - e_{fhi}\aleph u_{h,i} + \epsilon_{fi}\left[\Phi_{,if} + \aleph\Phi_{,i}\right] \tag{16}$$

It is convenient to use the contracted notation to introduce generalized piezoelectric vectors and tensors, which contain corresponding elastic and electric variables as follows:

$$U_H = \begin{cases} u_h & h = H = 1,2,3 \\ \Phi & H = 4 \end{cases} \tag{17}$$

$$Z_G = \begin{cases} t_g & g = G = 1,2,3 \\ q & G = 4 \end{cases} \tag{18}$$

$$C_{fGHi} = \begin{cases} C_{fghi}, & g = G = 1,2,3; h = H = 1,2,3 \\ e_{ifg}, & g = G = 1,2,3; H = 4 \\ e_{fhi}, & G = 4; \quad h = H = 1,2,3 \\ -\epsilon_{fi}, & G = 4; \quad H = 4 \end{cases} \tag{19}$$

Using the following Kronecker delta representation

$$\delta_{GH} = \begin{cases} \delta_{gh} & g = G = 1,2,3, \quad k = K = 1,2,3 \\ 0 & otherwise \end{cases} \tag{20}$$

The governing equations can be combined as follows:

$$L_{\mathrm{GH}} U_{\mathrm{H}} = \rho \delta_{GH} \ddot{U}_{\mathrm{H}} - \mathrm{B_G} \tag{21}$$

where

$$L_{\mathrm{GH}} = C_{f\mathrm{GH}i} \frac{\partial}{x_i} \frac{\partial}{x_f}$$

$$\mathrm{B_G} = \begin{cases} -\rho \ddot{u}_g - \mathrm{P}_0 \left(u_{g,f} - u_{f,g} \right) - \rho \omega^2 x_g + C_{fghi} \bar{\bar{u}} + \mathrm{e}_{ifg} \bar{\bar{\Phi}}, & g = G = 1,2,3 \\ \epsilon_{fi} \Phi_{,\mathrm{i}f} - \mathrm{e}_{fhi} \bar{\bar{u}} + \epsilon_{fi} \bar{\bar{\Phi}}, & G = 4 \end{cases}$$

$$\bar{\bar{u}} = \aleph u_{h,\mathrm{i}} \quad , \qquad \bar{\bar{\Phi}} = \Phi_{,if} + \aleph \Phi_{,i}$$

Now, we choose the fundamental solution U^*_{MH} as weighting function as follows

$$L_{GH} U^*_{MH}(x, \xi) = -\delta_{GM} \delta(x, \xi) \tag{22}$$

The weighted residual formula is integrated by parts twice to obtain the following piezoelectric reciprocity relation

$$\int_R \left(L_{\mathrm{GH}} \mathrm{U}_H U^*_{MG} - L_{\mathrm{GH}} U^*_{MH} \mathrm{U_G} \right) dR = \int_\Gamma \left(U^*_{MG} \mathrm{Z_G} - \mathrm{Z}^*_{MG} \mathrm{U_G} \right) d\Gamma \tag{23}$$

where

$$\mathrm{Z}^*_{MG} = C_{f\mathrm{GH}i} U^*_{MH,i} n_f$$

Making use of the sifting property, we obtain from equation (23) the piezoelectric representation formula

$$U_{\mathrm{M}}(\xi) = \int_\Gamma \left(U^*_{MG} \mathrm{Z_G} - \mathrm{Z}^*_{MG} \mathrm{U_G} \right) d\Gamma - \int_R U^*_{MG} (\rho \delta_{GH} \ddot{U}_{\mathrm{H}} - \mathrm{B_G}) dR \tag{24}$$

The DRBEM is employed in equation (24) to transform the domain integrals into boundary integrals, hence we may deduce the following piezoelectric dual reciprocity representation formula

$$U_H(\xi) = \int_\Gamma \left(U^*_{HG} \mathrm{Z_G} - \mathrm{Z}^*_{HG} \mathrm{U_G} \right) d\Gamma$$

$$+ \sum_{q=1}^{N} \left(U^q_{HN}(\xi) + \int_\Gamma \left(T^*_{HG} U^q_{GN} - \mathrm{U}^*_{HG} T^q_{GN} \right) d\Gamma \right) \alpha^{\mathrm{q}}_{\mathrm{N}} \tag{25}$$

Now the source term in equation (24) is approximated by a series of tensor functions f^{q}_{GN} and unknown coefficients $\alpha^{\mathrm{q}}_{\mathrm{N}}$ as follows

$$\rho\delta_{GH}\ddot{U}_{\mathrm{H}} - \mathrm{B}_{\mathrm{G}} \approx \sum_{q=1}^{N} f_{GN}^{\mathrm{q}}\alpha_{\mathrm{N}}^{\mathrm{q}} \tag{26}$$

Using the thin plate splines (TPS) as in Fahmy [27], we can write the particular solution of the displacement as follows

$$\mathrm{U}_{\mathrm{GN}}^{\mathrm{q}} = \begin{cases} -\dfrac{4}{\lambda^4}\left[K_0(\lambda r) + \log(r) - \dfrac{r^2\log r}{\lambda^2} - \dfrac{4}{\lambda^4}\right], & r > 0 \\ \dfrac{4}{\lambda^4}\left[\gamma + \log\left(\dfrac{\lambda}{2}\right)\right] - \dfrac{4}{\lambda^4}, & r = 0 \end{cases} \tag{27}$$

where K_0 is the Bessel function of the third kind of order zero and $\gamma = 0.5772156649015328$, which is known as Euler's constant, $r = \|x - \xi\|$ is the Euclidean distance between the field point x and the load point ξ.

Hence, the traction particular solution T_{GN}^{q} and the source function f_{GN}^{q} can be obtained by evaluating

$$T_{GN}^{q} = C_{f\mathrm{G}Hi}U_{HN,i}^{q}n_f\,, \quad L_{\mathrm{GH}}U_{HN}^{q} = f_{GN}^{\mathrm{q}} \tag{28}$$

According to Fahmy [35-38] and Fahmy et al. [39-42], the dual reciprocity boundary integral equation (25) can be written in the following system of equations

$$\zeta\breve{U}(t) - \eta\breve{\mathrm{T}}(\mathrm{t}) = \left(\zeta\breve{\mathrm{U}}(t) - \eta\breve{\mathrm{t}}(\mathrm{t})\right)\alpha(t) \tag{29}$$

where ζ, η are BEM system matrices, $\breve{U}$, $\breve{\mathrm{T}}$ contain the nodal values of the generalized displacements and fluxes, and $\breve{\mathrm{U}}$, $\breve{\mathrm{t}}$ contain the particular solutions

$$\begin{bmatrix} \rho\breve{\ddot{u}} - \rho\breve{b} \\ 0 \end{bmatrix} = \begin{bmatrix} F_{11} & F_{14} \\ F_{41} & F_{44} \end{bmatrix}\begin{bmatrix} \alpha_1 \\ \alpha_4 \end{bmatrix} \tag{30}$$

Now, the piezoelectric dual reciprocity representation formula can be written as

$$C_{HG}(\xi)\mathrm{U}_{\mathrm{G}}(\xi) + \mathrm{CPV}\int_{\Gamma} \mathrm{Z}_{HG}^{*}\mathrm{U}_{\mathrm{G}}\,d\Gamma = \int_{\Gamma} U_{HG}^{*}\mathrm{Z}_{\mathrm{G}}\,d\Gamma \tag{31}$$

Where CPV means the Cauchy Principal Value.

The coefficient vector $\alpha_{\mathrm{s}}(\mathrm{t})$ can be calculated by setting up a system of N equations from (26) using the point collocation procedure, which yield

$$\rho\breve{\ddot{u}} - \rho\breve{b} = \mathcal{F}_{11}\alpha_{\mathrm{s}}(\mathrm{t}) \tag{32}$$

where

$$\mathcal{F}_{11} = F_{11} - F_{14}F_{44}^{-1}F_{41} \tag{33}$$

$$\alpha_s(t) = \mathcal{F}^{-1}\left(\rho\ddot{\breve{U}}(t) - \breve{B}(t)\right) \tag{34}$$

$$\mathcal{F}^{-1} = \begin{cases} \mathcal{F}_{11}^{-1} & s = 1 \\ -\mathcal{F}_{44}^{-1}F_{41}\mathcal{F}_{11}^{-1} & s = 4 \\ 0 & \text{otherwise} \end{cases} \tag{35}$$

Substitution of (34) into (29) yields the system

$$M\ddot{\breve{U}}(t) + \zeta\breve{U}(t) = \eta\breve{T}(t) + \breve{\mathcal{B}}(t) \tag{36}$$

where the volume matrix V, piezoelectric mass matrix M and source vector $\breve{\mathcal{B}}(t)$ are as follows:

$$V = \left(\eta\check{\tau}(t) - \zeta\breve{U}(t)\right)\mathcal{F}^{-1}, \quad M = \rho V, \quad \breve{\mathcal{B}}(t) = V\breve{B}(t). \tag{37}$$

In order to solve system (36), the nodal vectors are subdivided into known and unknown parts denoted by the superscripts k and u.

$$\{U^k, T^u\} \in \Gamma_u, \qquad \{U^u, T^k\} \in \Gamma_T \tag{38}$$

The following matrix equation is obtained from Eq. (36).

$$\begin{bmatrix} M^{11} & M^{12} \\ M^{21} & M^{22} \end{bmatrix}\begin{bmatrix} \ddot{U}^k \\ \ddot{U}^u \end{bmatrix} + \begin{bmatrix} K^{11} & K^{12} \\ K^{21} & K^{22} \end{bmatrix}\begin{bmatrix} U^k(t) \\ U^u(t) \end{bmatrix} = \begin{bmatrix} \eta^{11} & \eta^{12} \\ \eta^{21} & \eta^{22} \end{bmatrix}\begin{bmatrix} T^k(t) \\ T^u(t) \end{bmatrix} + \begin{bmatrix} \mathcal{B}^1(t) \\ \mathcal{B}^2(t) \end{bmatrix} \tag{39}$$

The unknown fluxes $T^u(t)$ are obtained from the first row of matrix equation (24) and are expressed as follows.

$$\begin{aligned} T^u(t) = (\eta^{12})^{-1}\big[&M^{11}\ddot{U}^k(t) + M^{12}\ddot{U}^u(t) + K^{11}U^k(t) \\ &+K^{11}U^k(t) + K^{12}U^u(t) - \eta^{11}T^k(t) - \mathcal{B}^1(t)\big] \end{aligned} \tag{40}$$

Making use of Eq. (40), we can write the second row of matrix equation (39) as follows

$$M^u\ddot{U}^u(t) + K^uU^u(t) = Q^k(t) \tag{41}$$

where

$$Q^k(t) = \overline{\mathcal{B}}^k(t) + \eta^kT^k(t) - M^k\ddot{U}^k(t) - K^kU^k(t)$$

$$M^u = M^{22} - \eta^{22}(\eta^{12})^{-1}M^{12}$$

$$M^k = M^{21} - \eta^{22}(\eta^{12})^{-1}M^{11}$$

$$K^u = K^{22} - \eta^{22}(\eta^{12})^{-1}K^{12}$$

$$K^k = K^{21} - \eta^{22}(\eta^{12})^{-1}K^{11}$$

$$\eta^k = \eta^{21} - \eta^{22}(\eta^{12})^{-1}\eta^{11}$$

$$\overline{\mathcal{B}}^k(t) = \mathcal{B}^2(t) - \eta^{22}(\eta^{12})^{-1}\mathcal{B}^1(t)$$

We now split the system (41) into elastic and electric parts as follows:

$$\begin{bmatrix} M_{uu}^{u} & 0 \\ M_{\varphi u}^{u} & 0 \end{bmatrix}\begin{bmatrix} \ddot{u}^{u}(t) \\ \ddot{\varphi}^{u}(t) \end{bmatrix}+\begin{bmatrix} \mathrm{K}_{uu}^{u} & \mathrm{K}_{u\varphi}^{u} \\ \mathrm{K}_{\varphi u}^{u} & \mathrm{K}_{\varphi\varphi}^{u} \end{bmatrix}\begin{bmatrix} \mathrm{u}^{u}(\mathrm{t}) \\ \varphi^{u}(\mathrm{t}) \end{bmatrix}=\begin{bmatrix} \mathrm{Q}_{u}^{\mathrm{k}}(\mathrm{t}) \\ \mathrm{Q}_{\varphi}^{\mathrm{k}}(\mathrm{t}) \end{bmatrix} \tag{42}$$

The unknown electric potential φ^{u} can be obtained from the second row of Eq. (42) as follows

$$\varphi^{\mathrm{u}}(t)=\left(K_{\varphi\varphi}^{u}\right)^{-1}\left[\mathrm{Q}_{\varphi}^{\mathrm{k}}(\mathrm{t})-M_{\varphi u}^{u}\ddot{u}^{u}(t)-\mathrm{K}_{\varphi u}^{u}\mathrm{u}^{u}(\mathrm{t})\right] \tag{43}$$

With the use of Eq. (43) into the first row of Eq. (42) we obtain

$$\bar{M}^{u}\ddot{u}^{u}(t)+\bar{K}^{u}u^{u}(t)=\bar{Q}^{k}(t) \tag{44}$$

where

$$\bar{Q}^{k}(t)=Q_{u}^{k}(t)-\mathrm{K}_{u\varphi}^{u}\left(\mathrm{K}_{\varphi\varphi}^{u}\right)^{-1}\mathrm{Q}_{\varphi}^{\mathrm{k}}(\mathrm{t})$$

$$\bar{M}^{u}=M_{uu}^{u}-\mathrm{K}_{u\varphi}^{u}\left(\mathrm{K}_{\varphi\varphi}^{u}\right)^{-1}M_{\varphi u}^{u}$$

$$\bar{K}^{u}=K_{uu}^{u}-\mathrm{K}_{u\varphi}^{u}\left(\mathrm{K}_{\varphi\varphi}^{u}\right)^{-1}K_{\varphi u}^{u}$$

Now, writing equation (44) for the n+1th time step

$$\bar{M}^{u}\ddot{u}_{\mathrm{n+1}}^{u}+\bar{K}^{u}u_{\mathrm{n+1}}^{u}=\bar{Q}_{\mathrm{n+1}}^{\mathrm{k}} \tag{45}$$

where

$$\bar{Q}_{\mathrm{n+1}}^{\mathrm{k}}=\bar{\mathcal{B}}_{\mathrm{n+1}}^{\mathrm{k}}+\eta^{\mathrm{k}}\mathrm{T}_{\mathrm{n+1}}^{\mathrm{k}}-M^{k}\ddot{u}_{\mathrm{n+1}}^{\mathrm{k}}-K^{k}u_{\mathrm{n+1}}^{\mathrm{k}} \tag{46}$$

The Newmark time integration algorithm was used to reduce the system of ordinary differential equations (45) to an algebraic system. The displacements u_{n+1} and velocities $\dot{u}_{\mathrm{n+1}}$ used in this algorithm are approximated at time step n+1 as follows:

$$\dot{u}_{\mathrm{n+1}}\approx\dot{u}_{\mathrm{n}}+[(1-\delta)\ddot{u}_{\mathrm{n}}+\delta\ddot{u}_{\mathrm{n+1}}]\Delta\mathrm{t} \tag{47}$$

$$u_{n+1}\approx u_{n}+\dot{u}_{\mathrm{n}}\Delta\mathrm{t}+\left[\left(\frac{1}{2}-\alpha\right)\ddot{u}_{\mathrm{n}}+\alpha\ddot{u}_{\mathrm{n+1}}\right]\Delta\mathrm{t}^{2} \tag{48}$$

The acceleration at time step n+1 may be expressed from Equation (48) as:

$$\ddot{u}_{\mathrm{n+1}}\approx\frac{1}{\alpha\Delta\mathrm{t}^{2}}(u_{n+1}-u_{n})-\frac{1}{\alpha\Delta\mathrm{t}}\dot{u}_{\mathrm{n}}-\left(\frac{1}{2\alpha}-1\right)\ddot{u}_{\mathrm{n}} \tag{49}$$

Upon substitution of (49) into (45) we obtain the following algebraic system

$$\mathbb{R}u_{\mathrm{n+1}}^{\mathrm{u}}=\mathcal{M}_{\mathrm{n+1}} \tag{50}$$

where the stiffness matrix $\mathbb{R}$ and effective load vector $\mathcal{M}_{\mathrm{n+1}}$ are given by

$$\mathbb{R}=\frac{1}{\alpha\Delta\mathrm{t}^{2}}\bar{M}^{u}+\bar{K}^{u} \tag{51}$$

$$\mathcal{M}_{\mathrm{n+1}}=\bar{Q}_{\mathrm{n+1}}^{\mathrm{k}}+\bar{M}^{u}\left[\frac{1}{\alpha\Delta\mathrm{t}^{2}}u_{n}^{u}+\frac{1}{\alpha\Delta\mathrm{t}}\dot{u}_{n}^{u}+\left(\frac{1}{2\alpha}-1\right)\ddot{u}_{n}^{u}\right] \tag{52}$$

Once we have solved (50) for the unknown displacements at time step n+1, we can compute the accelerations and velocities from equations (49) and (47) respectively. Finally, the electric potential $\varphi^{\mathrm{u}}(t)$ can be obtained from (43) and the unknown generalized tractions $\mathrm{T}^{u}(\mathrm{t})$ can be determined using equation (40).

4. Numerical results and discussion

With the view of illustrating the numerical results calculated by method presented in this paper, the material chosen for the plate is the piezoelectric ceramic Lead Zirconate Titanate (PZT), and the physical data for which is given as follows:

The elasticity tensor C , piezoelectric tensor e and relative permittivity ϵ^{rel}

$$C_{fghi} = \begin{pmatrix} 107.6 & 63.10 & 63.90 & 0.000 & 0.000 & 0.000 \\ 63.10 & 107.6 & 63.90 & 0.000 & 0.000 & 0.000 \\ 63.90 & 63.90 & 100.4 & 0.000 & 0.000 & 0.000 \\ 0.000 & 0.000 & 0.000 & 19.60 & 0.000 & 0.000 \\ 0.000 & 0.000 & 0.000 & 0.000 & 19.60 & 0.000 \\ 0.000 & 0.000 & 0.000 & 0.000 & 0.000 & 22.20 \end{pmatrix} \tag{53}$$

$$e = \begin{pmatrix} 0.00 & 0.00 & 0.00 & 0.00 & 12.0 & 0.00 \\ 0.00 & 0.00 & 0.00 & 12.0 & 0.00 & 0.00 \\ -9.6 & -9.6 & 15.1 & 0.00 & 0.00 & 0.00 \end{pmatrix} \tag{54}$$

$$\epsilon^{\mathrm{rel}} = \begin{pmatrix} 1936 & 0.00 & 0.00 \\ 0.00 & 1936 & 0.00 \\ 0.00 & 0.00 & 2109 \end{pmatrix} \tag{55}$$

The present work should be applicable to any anisotropic FGPP deformation problem. The application is for purpose of illustration; we do not intend to validate the results in a quantitative way because we have no experimental data at hand; this may be justified because our objective is to introduce a viable numerical technique for studying a model rather than to study any physical behaviors of it. Such a technique was discussed in Fahmy [43] who solved the special case from this study in 2D in the absence of rotation and initial stress. To achieve better efficiency than the technique described in Fahmy [43], we use thin plate splines into a code, which is proposed in the current study. We extend the study of Fahmy [43], to solve 3D in the presence of rotation and initial stress. Thus, it is perhaps not surprising that the numerical values obtained here are in excellent agreement with those obtained by Fahmy [43].

The results of calculations are presented in Figs. 2–4. Comparison of the results is presented graphically for the following different cases: the solid line represents the solution in absence of initial stress ($\mathrm{P} = 0$) and rotation ($\omega = 0$), the dashed line represents the solution in the

presence of initial stress $(P = 0.5)$ and in the absence of rotation $(\omega = 0)$, the dotted line represents the solution in the absence of initial s tress $(P = 0)$ and in the presence of rotation $(\omega = 0.5)$ and the dashed-dotted line represents the solution in presence of initial stress $(P = 0.5)$ and rotation $(\omega = 0.5)$. It can be seen from these figures that the effect of initial stress and rotation is very pronounced.

To evaluate the influence of the inhomogeneity on the displacements in an anisotropic FGPP, the inhomogeneity parameter is taken to be $m = 0$ for the homogeneous plate, we assume that $m = 1$ for functionally graded plate. The computed results are presented graphically in Figs. 5-7, the figures show the difference between homogeneous and functionally graded plates.
In the special case under consideration, the results are plotted in Figs. 8–10 to show the validity of the DRBEM. These results obtained with the DRBEM have been compared graphically with those obtained using the Meshless Local Petrov–Galerkin (MLPG) method of Stanak et al. [45] and also the results obtained using the Peano-Baker Series (PBS) method of Liu et al. [46] are shown graphically in the same figures to confirm the validity of the proposed method. It can be seen from these figures that the DRBEM results are in excellent agreement with the results obtained by MLPG and PBS methods, thus confirming the accuracy of the DRBEM.

ACKNOWLEDGEMENT

The author would like to express his deepest gratitude to the Institute of Consulting Research and Studies (ICRS) at Umm Al-Qura University, Makkah, Saudi Arabia, for supporting and encouraging him during the development of this paper.

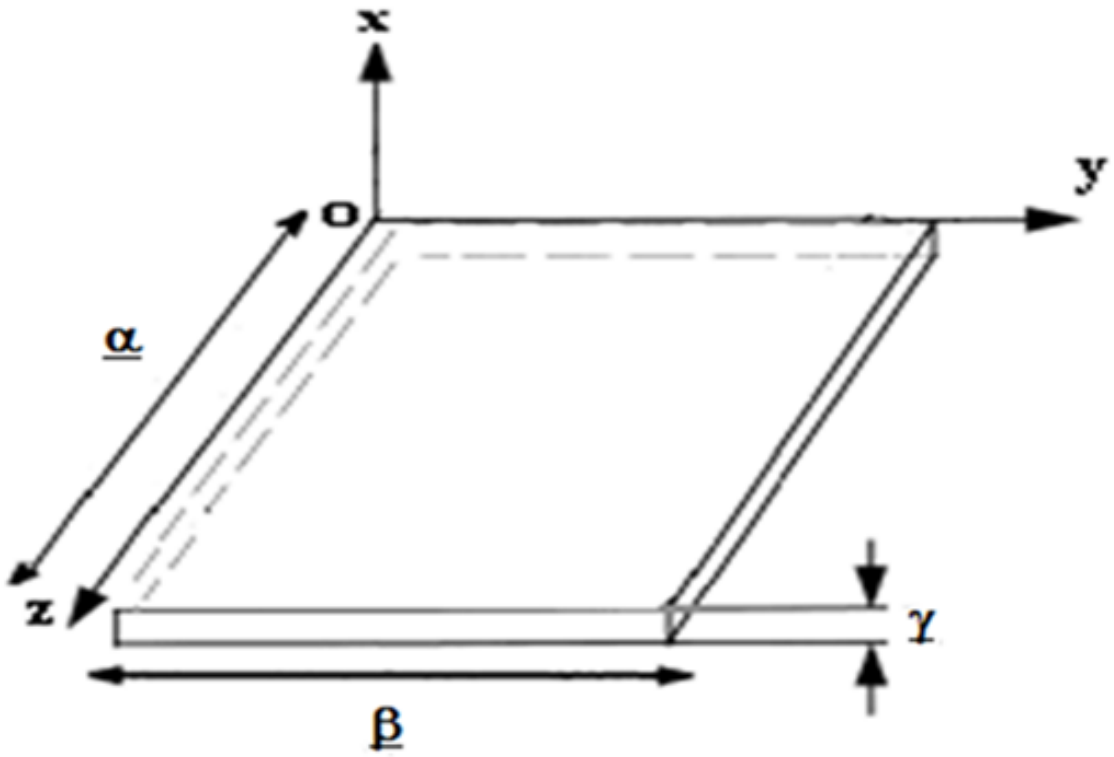

Fig. 1. The coordinate system of the FGPP.

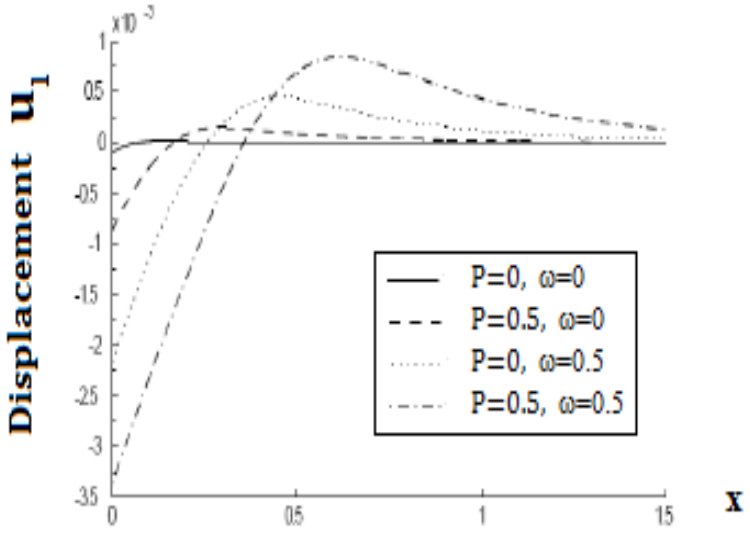

Fig. 2. Variation of the displacement u_1 with x coordinate.

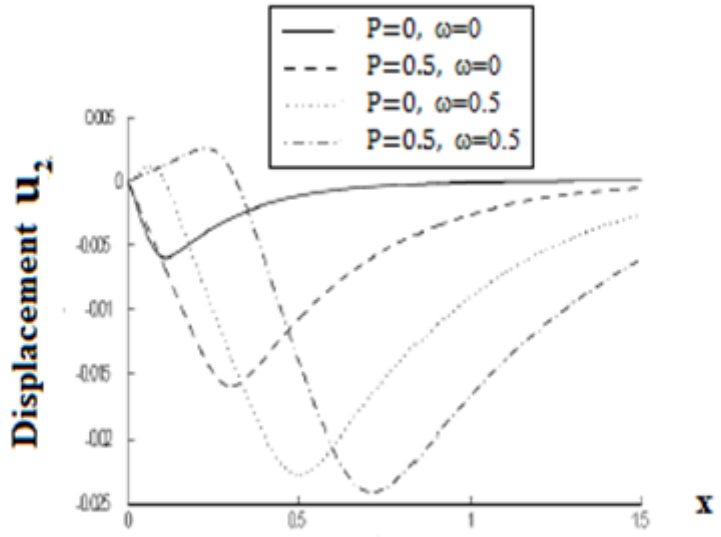

Fig. 3. Variation of the displacement u_2 with x coordinate.

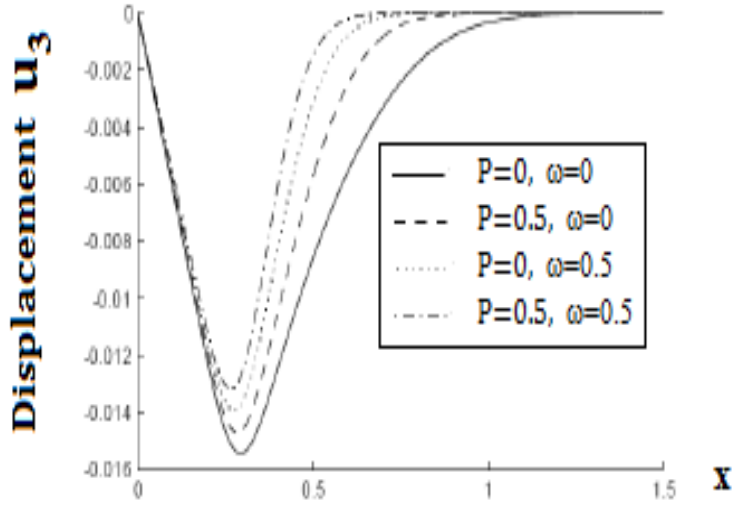

Fig. 4. Variation of the displacement u_3 with x coordinate.

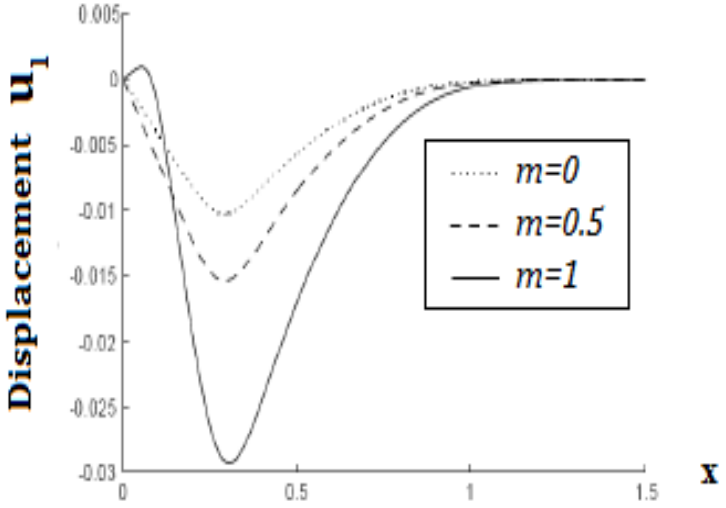

Fig. 5. Variation of the displacement u_1 with x coordinate.

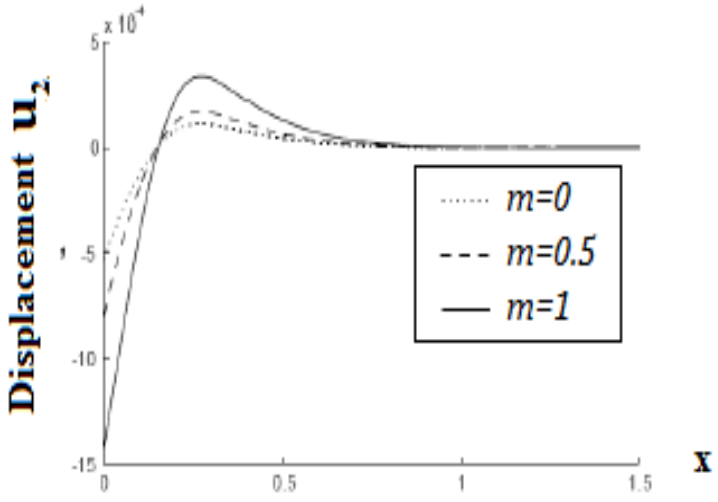

Fig. 6. Variation of the displacement u_2 with x coordinate.

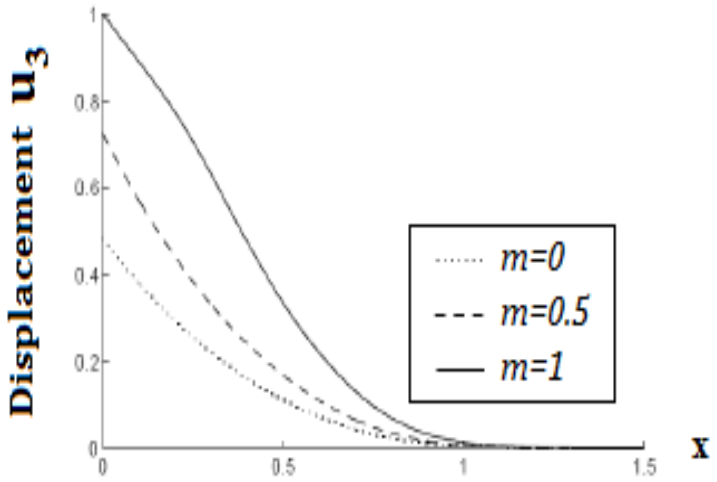

Fig. 7. Variation of the displacement u_3 with x coordinate.

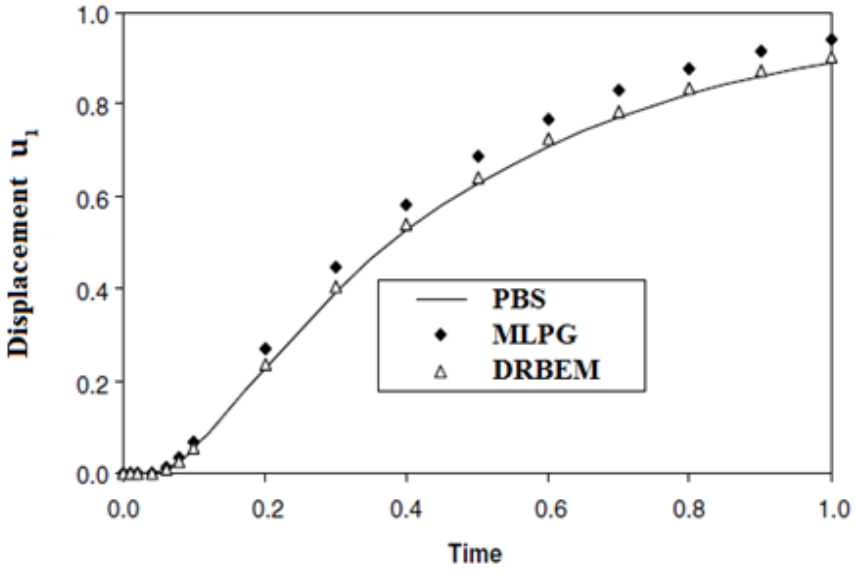

Fig. 8. Variation of the Displacement u_1 with time for three methods.

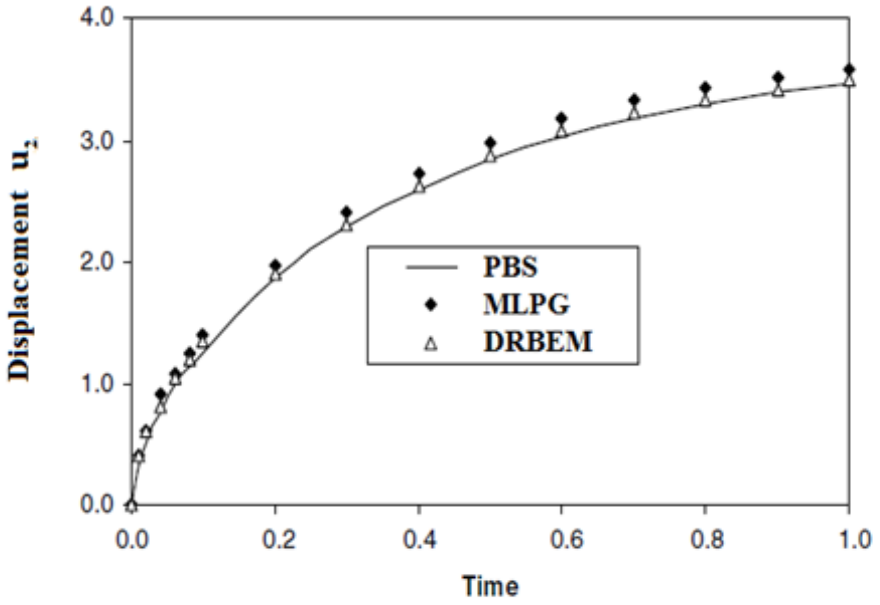

Fig. 9. Variation of the displacement u_2 with time for three methods.

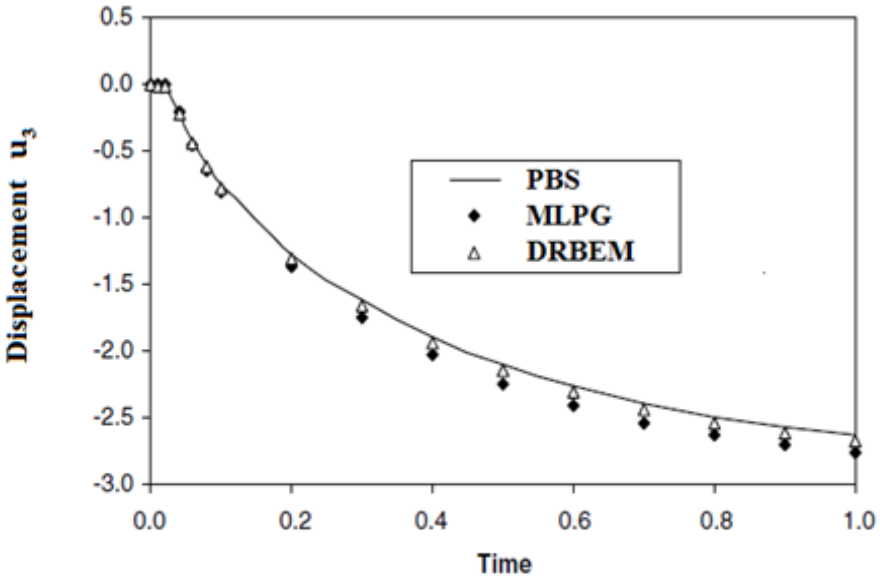

Fig. 10. Variation of the displacement u_3 with time for three methods.

REFERENCES

[1] Z. Suo, C.M. Kuo, D.M. Barnett, J.R. Willis, Fracture mechanics for piezoelectric ceramics. Journal of the Mechanics and Physics of Solids, 40, 739–65, 1992.

[2] E.A. Pan, BEM analysis of fracture mechanics in 2D anisotropic piezoelectric solids. Engineering Analysis with Boundary Elements, 23, 67–76, 1999.

[3] B. Jin, Z. Zhong, A moving mode-III crack in functionally graded piezoelectric material: permeable problem," Mechanics Research Communications, 29, 217–24, 2002.

[4] T.Y. Zhang, M.H. Zhao, P. Tong, Fracture of piezoelectric ceramics. Advances in Applied Mechanics, 38, 147–289, 2002.

[5] S. Lin, F. Narita, Y. Shindo [2003] "Electroelastic analysis of a penny-shaped crack in a piezoelectric ceramic under mode I loading. Mechanics Research Communications 30, 371–86, 2003.

[6] D.N. Fang, Y.P. Wan, A.K. Soh, Magnetoelastic fracture of soft ferromagnetic Materials. Theoretical and Applied Fracture Mechanics, 42, 317–34, 2004.

[7] A.N. Abd-Alla, F.A. Alsheikh [2009a] "Reflection and refraction of plane quasi-longitudinal waves at an interface of two piezoelectric media under initial stresses," Archive of Applied Mechanics 79, 843–857, 2009.

[8] A.N. Abd-Alla, F.A. Al-sheikh [2009b] "The effect of the initial stresses on the reflection and transmission of plane quasi-vertical transverse waves in piezoelectric materials," World Academy of Science, Engineering and Technology 50, 660-668, 2009.

[9] M. Kuna [2010] "Fracture mechanics of piezoelectric materials – where are we right now?" Eng Fract Mech 77(2), 309–26, 2010.

[10] M. Zaman, Z. Yan, L. Jiang [2010] " Thermal effect on the bending behavior of curved functionally graded piezoelectric actuators," International Journal of Applied Mechanics 02(04), 787-805, 2010.

[11] X.C. Zhong, K.S. Zhang, Electroelastic analysis of an electrically dielectric Grif!th crack in a piezoelectric layer. International Journal of Engineering Science, 48, 612–23, 2010.

[12] A.H. Akbarzadeh, M.H. Babaei and Z.T. Chen, Thermopiezoelectric analysis of a functionally graded piezoelectric medium. International Journal of Applied Mechanics, 3, 47-68, 2011.

[13] G. Davì, A. Milazzo, A regular variational boundary model for free vibrations of magneto-electro-elastic structures. Engineering Analysis with Boundary Elements, 35, 303-312, 2011.

[14] A.N. Abd-Alla, F.A. Al-Sheikh, A.Y. Al-Hossain, The reflection phenomena of quasi-vertical transverse waves in piezoelectric medium under initial stresses. Meccanica, 47, 731-744, 2012.

[15] A.N. Abd-Alla, N.A. Askar, Calculation of bulk acoustic wave propagation velocities in trigonal piezoelectric smart materials. Applied Mathematics and Information Sciences 8, 1-8, 2014.

[16] A. Alibeigloo, K.M. Liew [2015] "Elasticity Solution of Free Vibration and Bending Behavior of Functionally Graded Carbon Nanotube-Reinforced Composite Beam with

Thin Piezoelectric Layers Using Differential Quadrature Method," International Journal of Applied Mechanics 7(1), 1550002, 2015.

[17] M. Rafiee, X.Q. He, S. Mareishi and K.M. Liew, Nonlinear Response of Piezoelectric Nanocomposite Plates: Large Deflection, Post-Buckling and Large Amplitude Vibration. International Journal of Applied Mechanics, 7, 1550074, 2015.

[18] D. Nardini, C.A. Brebbia [1982] "A new approach to free vibration analysis using boundary elements, in: C. A. Brebbia (Eds.), Boundary elements in engineering, Springer, Berlin, 312-326, 1982.

[19] C.A. Brebbia, J.C.F. Telles and L. Wrobel, Boundary element techniques in Engineering. (Springer-Verlag, New York), 1984.

[20] L.C. Wrobel, C.A. Brebbia, The dual reciprocity boundary element formulation for nonlinear diffusion problems. Computer Methods in Applied Mechanics and Engineering, 65, 147-164, 1987.

[21] P.W. Partridge, C.A. Brebbia [1990] "Computer implementation of the BEM dual reciprocity method for the solution of general field equations. Communications in Applied Numerical Methods, 6, 83-92, 1990.

[22] P.W. Partridge, L.C. Wrobel, The dual reciprocity boundary element method for spontaneous ignition. International Journal for Numerical Methods in Engineering, 30, 953–963, 1990.

[23] J.H. Frijns, S.L. de Snoo and R. Schoonhoven, Improving the accuracy of the boundary element method by the use of second-order interpolation functions. IEEE Transactions on Biomedical Engineering, 47, 1336-1346, 2000.

[24] L. Gaul, M. Kögl and M. Wagner [2003] "Boundary element methods for engineers and scientists," (Springer-Verlag, Berlin), 2003.

[25] M.A. Fahmy, Application of DRBEM to non-steady state heat conduction in non-homogeneous anisotropic media under various boundary elements. Far East Journal of Mathematical Sciences, 43, 83-93, 2010.

[26] M.A. Fahmy, A time-stepping DRBEM for magneto-thermo-viscoelastic interactions in a rotating nonhomogeneous anisotropic solid. Int. J. Appl. Mech., 3, 1-24, 2011.

[27] M.A. Fahmy, Influence of inhomogeneity and initial stress on the transient magneto-thermo-visco-elastic stress waves in an anisotropic solid. World Journal of Mechanics, 1, 256-265, 2011.

[28] M.A. Fahmy, A time-stepping DRBEM for the transient magneto-thermo-visco-elastic stresses in a rotating non-homogeneous anisotropic solid. Engineering Analysis with Boundary Elements, 36, 335-345, 2012.

[29] M.A. Fahmy, Numerical modeling of transient magneto-thermo-viscoelastic waves in a rotating nonhomogeneous anisotropic solid under initial stress. International Journal of Modeling, Simulation, and Scientific Computing, 3, 125002, 2012.

[30] M.A. Fahmy, Transient magneto-thermo-elastic stresses in an anisotropic viscoelastic solid with and without moving heat source. Numer. Heat Transfer, Part A., 61, 547-564, 2012.

[31] M.A. Fahmy, Transient magneto-thermoviscoelastic plane waves in a non-homogeneous anisotropic thick strip subjected to a moving heat source, Applied Mathematical Modelling, 36, 4565-4578, 2012.

[32] M.A. Fahmy, Transient magneto-thermo-viscoelastic stresses in a rotating nonhomogeneous anisotropic solid with and without a moving heat source. Journal of Engineering Physics and Thermophysics, 85, 874-880, 2012.

[33] M.A. Fahmy, The DRBEM solution of the generalized magneto-thermo-viscoelastic problems in 3D anisotropic functionally graded solids. I. Idelsohn, M. Papadrakakis, B. Schrefler Eds. 5th International conference on coupled problems in science and engineering (Coupled Problems 2013), Ibiza, Spain, pp. 862-872, June 17-19, 2013.

[34] M.A. Fahmy, Generalized Magneto-Thermo-Viscoelastic Problems of Rotating Functionally Graded Anisotropic Plates by the Dual Reciprocity Boundary Element Method. Journal of Thermal Stresses, 36, 284-303, 2013.

[35] M.A. Fahmy, A Three-Dimensional Generalized Magneto-Thermo Viscoelastic Problem of a Rotating Functionally Graded Anisotropic Solids with and without Energy Dissipation. Numerical Heat Transfer, Part A: Applications, 63, 713–733, 2013.

[36] M.A. Fahmy, Implicit–Explicit Time Integration DRBEM for Generalized Magneto-Thermoelasticity Problems of Rotating Anisotropic Viscoelastic Functionally Graded Solids. Engineering Analysis with Boundary Elements, 37, 107-115, 2013.

[37] M.A. Fahmy, A Comuputerized DRBEM model for generalized magneto-thermo-viscoelastic stress waves in functionally graded anisotropic thin film/substrate structures. Latin American Journal of solids and structures, 11, 386 – 409, 2014.

[38] M.A. Fahmy M. A. [2014b] "A 2D Time Domain DRBEM Computer Model for Magneto-Thermoelastic Coupled Wave Propagation Problems. International Journal of Engineering and Technology Innovation, 4, 138-151, 2014.

[39] M.A. Fahmy, A.M. Salem, M.S. Metwally and M.M. Rashid, Computer Implementation of the DRBEM for Studying the Generalized Thermoelastic Responses of Functionally Graded Anisotropic Rotating Plates with One Relaxation Time. International Journal of Applied Science and Technology, 3, 130-140, 2013.

[40] M.A. Fahmy, A.M. Salem, M.S. Metwally and M.M. Rashid, Computer Implementation of the Drbem for Studying the Classical Uncoupled Theory of Thermoelasticity of Functionally Graded Anisotropic Rotating Plates. International Journal of Engineering Research and Applications, 3, 1146-1154, 2013.

[41] M.A. Fahmy, A.M. Salem, M.S. Metwally and M.M. Rashid, Computer Implementation of the DRBEM for Studying the Classical Coupled Thermoelastic Responses of Functionally Graded Anisotropic Plates. Physical Science International Journal, 4, 674-685, 2014.

[42] M.A. Fahmy, A.M. Salem, M.S. Metwally and M.M. Rashid, Computer Implementation of the DRBEM for Studying the Generalized Thermo Elastic Responses of Functionally Graded Anisotropic Rotating Plates with Two Relaxation Times. British Journal of Mathematics & Computer Science, 4, 1010-1026, 2014.

[43] M.A. Fahmy, Boundary Element Solution of 2D Coupled Problem in Anisotropic Piezoelectric FGM Plates. Proceedings of the, B. Schrefler, E. Oñate and M. Papadrakakis eds. 6th International Conference on Computational Methods for Coupled Problems in

Science and Engineering (Coupled Problems 2015), Venice. Italy, pp. 382-391, May 18-20, 2015.

[44] M.A. Fahmy, A comuputerized DRBEM model for 3D dynamic coupled problems in anisotropic piezoelectric FGM plates, Presented in 2nd International Conference on New Horizons in Basic and Applied Science (ICNHBAS 2015), Hurghada, Egypt, August 1-6, 2015.

[45] P. Stanak, J. Sladek, V. Sladek, A. Tadeu, Three-Dimensional Meshless Modelling of Functionally Graded Piezoelectric Sensor. in Mechatronics 2013, ed. T. Březina and R. Jabloński (Springer International Publishing Switzerland), pp. 425-432.

[46] W. Liu, S. Ma, H. Wu, Three-dimensional analysis of functionally graded piezoelectric plate with arbitrarily distributed material properties. Journal of Wuhan University of Technology-Mater. Sci. Ed., 29, 712-720, 2014.